ELSEVIER

International Journal of Heat and Fluid Flow 20 (1999) 95–104

International Journal of HEAT AND FLUID FLOW

A physical model for bypass transition

Mark W. Johnson *, Ali H. Ercan [1]

Department of Engineering, The University of Liverpool, Liverpool, L693GH, UK

Received 24 March 1998; accepted 2 October 1998

Abstract

A new method of predicting boundary layer transition is presented which models the near wall velocity fluctuations induced in the laminar layer through pressure fluctuations associated with the freestream turbulence. These near wall velocity fluctuations are then assumed to develop into turbulent spots when their amplitude exceeds a threshold value. A relationship for the near wall velocity frequency spectra is also established, which indicates an increasing bias towards low frequencies as the skin friction coefficient for the boundary layer decreases. This result suggests that the dependence of transition on the turbulent length scale is greatest at low freestream turbulence levels. This transition model is incorporated in a conventional boundary layer integral technique and is used to predict eight of the ERCOFTAC test cases and measurements of Gostelow and co-workers. The model is demonstrated to predict the development of the boundary layer through transition reasonably accurate for all the test cases. The sensitivity of start of transition to the turbulent length scale at low freestream turbulence levels is also demonstrated. The model is also able to predict the evolution of measured intermittency more accurately than the Narasimha empirical correlation.

Notation

a, b, c	empirical coefficients in Eq. (1)
C_f	skin friction coefficient
e	near wall power spectral density
E	freestream power spectral density
f	fluctuation frequency
G	gain or ratio between near wall and freestream turbulence levels for a particular frequency
H	$(=\delta^*/\theta)$ shape factor
ℓ	near wall integral length scale
L	freestream integral length scale
n	spot generation rate per unit time per unit span
N	spots per unit span
P	probability distribution
Re_L	Reynolds number based on freestream integral length scale
Re_x	Reynolds number based on streamwise distance
Re_θ	momentum thickness Reynolds number
Tu	freestream turbulence level
u	local time mean velocity
u'	local instantaneous fluctuating velocity
u'_m	local fluctuating velocity minima
$\overline{u}'_f$	local r.m.s. velocity in a particular frequency band
$\overline{u}'$	local r.m.s. velocity
u_{yo}	velocity gradient at the wall
U	freestream time mean velocity
$\overline{U}'$	freestream r.m.s. velocity
$\overline{U}'_f$	freestream r.m.s. velocity in a particular frequency band
x	streamwise distance from leading edge
x_o	streamwise distance between grid and plate leading edge
x_s	Narasimha start of transition position
y	normal distance from plate
z	velocity fluctuation minima per local integral wavelength
α	spot spreading half angle
γ	intermittency
δ	boundary layer thickness
δ^*	displacement thickness
θ	momentum thickness
λ	$(=\delta^2/\nu)(\mathrm{d}U/\mathrm{d}x)$ Pohlhausen parameter
λ_θ	$(=\Theta/\nu)(\mathrm{d}U/\mathrm{d}x)$ pressure gradient parameter
ν	kinematic viscosity
ξ	Narasimha dimensionless distance

Subscripts

l	laminar
NW	near wall $(y/\delta = 0.1)$
t	turbulent

1. Introduction

Previous boundary layer transition studies (Mayle (1991)) have identified two distinct transition mechanisms. The first, which occurs at freestream turbulence levels less than about 1%, is due to the amplification of Tollmien–Schlichting (T-S)

* Corresponding author. E-mail: em22@liverpool.ac.uk.

[1] Current address: Mechanical Engineering Department, Cumhurijet University, Sivas. Turkey

0142-727X/99/$ – see front matter
PII: S0142-727X(98)10051-6

waves. At higher freestream turbulence levels, where there is little evidence of these T-S waves transition takes place through a second bypass mechanism. Only bypass transition is pertinent in gas turbine engines.

Current boundary layer integral techniques predict start of transition and transition length through empirical correlations, e.g., Abu-Ghannam and Shaw (1980) and Solomon et al. (1995). Prediction of transitional boundary layers has also been achieved using Computational Fluid Dynamics, e.g., Steelant and Dick (1994), but current turbulence models, which are also essentially empirical, are generally found to be inadequate for this purpose. Good prediction may be achieved using Direct Numerical Simulation (Voke and Yang (1993)), where the full unsteady Navier–Stokes equations are solved on a fine computational grid. The evolution of individual turbulent eddies is thus predicted. The technique is however computationally very expensive and is therefore unsuitable for general gas turbine design purposes.

At low freestream turbulence levels and under adverse pressure gradients, where T-S waves lead to transition, it has been recognised that, if the amplitude of the wave is large enough, each cycle of the wave results in the generation of a single turbulent spot. Walker and Gostelow (1990) determined a minimum possible transition length through this assumption. The transition length was then predicted by multiplying the minimum transition length by an empirical factor (greater than 1) to correct for the fact that not all cycles of the T-S wave would have sufficient amplitude to initiate a spot. For bypass transition, a single T-S frequency is not observed within the boundary layer, but rather a complete spectra of frequencies. However, it is not unreasonable to adopt Walker's model and propose that every minimum of sufficient amplitude within the velocity signal will initiate a turbulent spot.

The objective of the current work is to develop such a model and to adopt it within a boundary layer integral technique in order to compute transitional boundary layers.

2. Experimental procedure

The wind tunnel and instrumentation used in obtaining the experimental data presented in this paper, are described in detail by Fasihfar and Johnson (1992). The measurements were made using hot wire anemometry within laminar boundary layers developed on a flat plate. A range of adverse and favourable streamwise pressure gradients was used with freestream turbulence energy levels varying between 0.5% and 5%.

3. Transition model

Johnson (1994) suggested that a turbulent spot is initiated in a laminar boundary layer when a local instantaneous separation of the flow occurs. The mechanism for spot initiation is consistent with recent Direct Numerical Simulation calculations, Voke (1995), which show, within the transition inception region, instantaneous velocity distributions near the wall, characteristic of small transient separation bubbles. Johnson (1994) was also able to show that a local separation of the flow takes place when the local instantaneous velocity in the near wall region drops below 50% of the local time mean velocity. The spot formation rate can therefore be predicted if statistical information on the number and depth of the minima within the near wall velocity signal can be derived. In order to achieve this the response of laminar boundary layers to freestream turbulence must be considered.

3.1. Boundary layer response to freestream turbulence

A number of possible mechanisms exist through which turbulence can enter the laminar boundary layer from the freestream. Velocity perturbations could be convected along streamlines or can 'diffuse' into the boundary layer from the freestream. However, if these perturbations were to convect at the fluid velocity within the boundary layer, strong gradients in fluctuation velocity would rapidly develop because of the strong variation in convection rate within the shear layer and hence the perturbations would be quickly dissipated by viscosity. Furthermore, the strength of the perturbations at any streamwise location would depend on the manner in which they had developed (i.e., their history). This would mitigate the success of empirical correlations based on local parameters (i.e, neglecting history). If the near wall velocity fluctuations depend primarily on the local turbulence and pressure gradient in the freestream, a more plausible mechanism than convection or diffusion is that the near wall velocity perturbations result from the unsteady pressure field generated by the freestream turbulence. This mechanism has recently been modelled by Mayle and Schulz (1996) and has been shown to give excellent predictions of the response of the laminar boundary layer to freestream turbulence. In the current model, the unsteady pressure field is also assumed to be responsible for generating near wall velocity fluctuations. Fig. 1 shows the ratio of the local to freestream turbulence levels (gain) in six frequency bands through a typical laminar boundary layer.

It can be seen that for the highest frequency bands, the gain is approximately one throughout the boundary layer indicating that the local and freestream turbulence levels are similar. However, for the lowest frequency bands the gain rises to around 40, indicating that these low frequencies become dominant in the velocity signal close to the wall. The other noticeable feature is that the spectra are invariant (constant gain) for y/δ values up to approximately 0.3. Throughout this paper this region will be referred to as the 'near-wall region' and near wall flow quantities are those measured or predicted at $y/\delta = 0.1$. The near wall gain is shown for a number of different zero pressure gradient boundary layers in Fig. 2. For dimensionless frequencies greater than 0.1 the results are very similar, but for low frequencies the ratio increases with decreasing C_f. The results for these boundary layers can be reasonably represented by

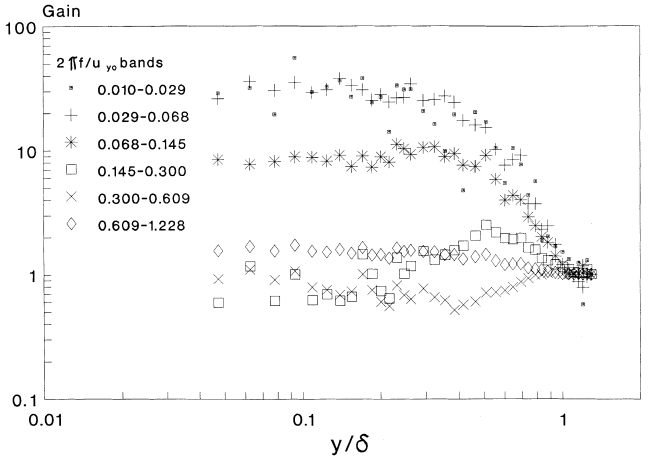

Fig. 1. Amplification of six frequency bands through a laminar boundary layer.

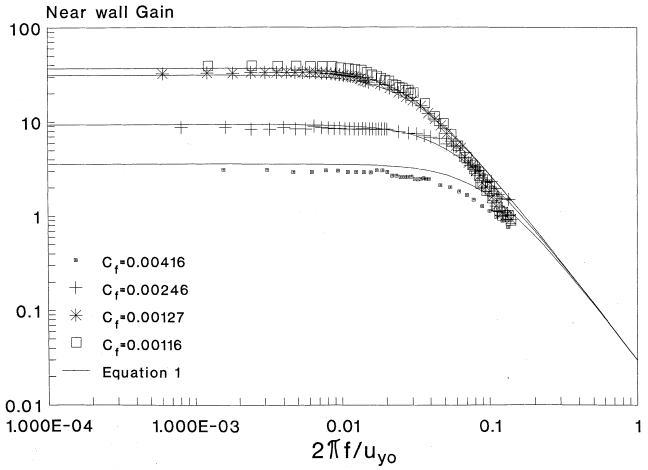

Fig. 2. Near wall amplification as a function of frequency.

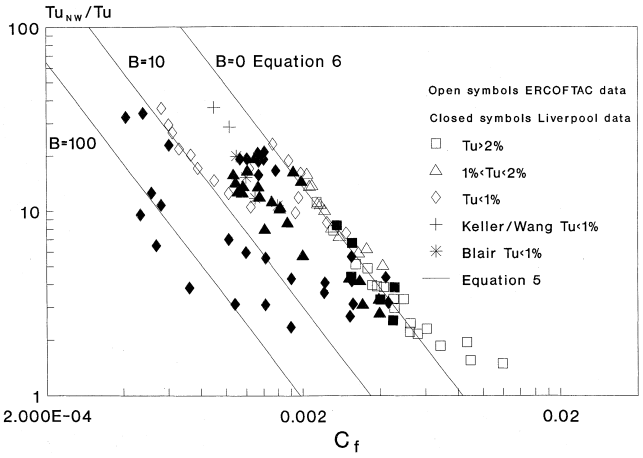

Fig. 3. Ratio of near wall to freestream turbulence levels for favourable zero and adverse pressure gradient laminar boundary layers.

$$G = \frac{\bar{u}'_f}{u}\frac{U}{\bar{U}'_f} = \frac{a}{C_f^c + (2\pi b f/u_{yo})^2}. \tag{1}$$

It is now assumed that the freestream turbulence is isotropic and can be represented, Hinze (1959), by

$$\frac{4\bar{U}'^2 L}{EU} = 1 + \left(\frac{2\pi f L}{U}\right)^2, \tag{2}$$

where L is the freestream integral length scale and E the Power Spectral Density.

The near wall spectral density e is then given by

$$e = \left(\frac{\bar{u}'_f}{\bar{U}'_f}\right)^2 E = G^2\left(\frac{\bar{U}'}{U}\right)^2\left(\frac{u}{U}\right)^2 \frac{4UL}{\left(1+\left(\frac{2\pi f L}{U}\right)^2\right)} \tag{3}$$

and hence the near wall local turbulence level Tu_{NW} is given by

$$\mathrm{Tu}_{NW}^2 = \int_0^\infty \frac{e\,\mathrm{d}f}{u^2} = \frac{4a^2\mathrm{Tu}^2}{C_f^{2c}}\int_0^\infty \frac{\mathrm{d}F}{(1+(BF)^2)^2(1+F^2)}, \tag{4}$$

where

$$F = \frac{2\pi f L}{u},\quad B = \frac{2b}{Re_L C_f^{(1+c/2)}},\quad \mathrm{Re}_L = \frac{UL}{\nu}$$

and so the ratio of near wall to freestream turbulence levels

$$\left(\frac{\mathrm{Tu}_{NW}}{\mathrm{Tu}}\right) = \frac{a}{C_f^c}(B+1)\left(\frac{B}{2}+1\right)^{1/2}. \tag{5}$$

It therefore follows that if B is small (less than approximately 0.1),

$$\frac{\mathrm{Tu}_{NW}}{\mathrm{Tu}} = aC_f^{-c} \tag{6}$$

and hence is independent of the freestream length scale. This is true if the majority of the freestream turbulent energy is for the low frequencies which have the highest gain in Fig. 2. This is generally the case for high freestream turbulence levels where both the length scale and C_f are comparatively large and hence B is small. Fig. 3 confirms this, as the high freestream Tu results fall close to a single line represented by Eq. (6). The results for turbulence levels less than approximately 1.5%, where B is larger, lie below this line. A least rms error curve fitting technique was used with the data in this figure to obtain the coefficient values

$$a = 1.595\times10^{-4},\quad b = 0.015,\quad c = 1.827.$$

3.2. Near wall velocity signal

The near wall integral length scale ℓ is evaluated, from its definition, through the equation

$$\int_0^{U/\ell} e\,\mathrm{d}f = \frac{1}{2}\int_0^\infty e\,\mathrm{d}f. \tag{7}$$

Substituting for e from Eq. (3) and integrating, this becomes

$$\frac{2}{\pi}\frac{2}{B^2-1}\left[\frac{1}{4}\sin 2\phi + \frac{\phi}{2}\right] + \frac{2}{\pi(B^2-1)^2}\left[\mathrm{Tan}^{-1}\frac{L}{\ell} - B\phi\right] = \frac{B+2}{4(B+1)^2}, \tag{8}$$

where $\phi = \mathrm{Tan}^{-1}(BL/\ell)$.

This equation can be solved numerically to obtain ℓ/L for any value of B.

The near wall velocity signal was synthesised from the power spectral density for a range of B values. These signals were then analysed to obtain statistical information for the minima. The number of minima per local wavelength z as a function of the length scale ratio (ℓ/L) is found to be closely represented by

$$z = 3.2 - 2.5\exp(-0.043\ell/L). \tag{9}$$

The instantaneous velocities have a normal distribution about the mean value and the minima have a distribution

$$\left(\frac{u'_m}{\bar{u}'}\right)^2 \exp\left(-\frac{1}{2}\left(\frac{u'_m}{\bar{u}'}\right)^2\right).$$

If Johnson's criterion (Johnson, 1994) is now adopted, namely that any minima where $u'_m/u < 0.5$ will lead to the generation of a turbulent spot, it follows that the proportion of minima P which will generate spots is given by

$$P = \frac{1}{4}\sqrt{\frac{1}{2\pi}}\int_\infty^{u/2\bar{u}'}\left(\frac{u}{\bar{u}'}\right)^2\exp\left(-\frac{1}{8}\left(\frac{u}{\bar{u}'}\right)^2\right)\mathrm{d}\left(\frac{u}{\bar{u}'}\right). \tag{10}$$

Assuming the freestream turbulence is convected at the freestream velocity U, then the spot generation rate per unit time per unit area of the surface is $PU(z/\ell)^3$.

3.3. Turbulent spot development

Gostelow et al. (1995) have recently provided correlations for spot trailing edge and leading edge velocities (U_{TE} and U_{LE}) spreading half angle (α) and propagation parameter (σ) in favourable and adverse pressure gradients as shown in Fig. 4. When these correlations were used in the current model, transition length was overpredicted when transition occurred in a strong adverse pressure gradient. This was believed to be because the correlations for α and σ limited the values to 32° and 0.8, respectively for adverse pressure gradients. For this reason alternative correlations were formulated. If the laminar boundary layer is assumed to have a Pohlhausen velocity profile, the trailing and leading edge velocities are well represented by the velocities existing at $y/\delta = 0.27$ and 0.57, respectively, as shown in Fig. 4. Therefore

$$\frac{U_{TE}}{U} = 0.506 + 0.0175\lambda$$

and

$$\frac{U_{TE}}{U} = 0.875 + 0.00755\lambda, \tag{11}$$

where $\lambda = \lambda_\theta/(\theta/\delta)^2$.

The spreading half angle α can be represented by

$$\alpha = \mathrm{Tan}^{-1}\left(\frac{0.242(U_{LE} - U_{TE})}{U_{TE}(1+\lambda/12)^2}\right) \tag{12}$$

and the propagation parameter σ can then be evaluated as

$$\sigma = \left(\frac{U}{U_{TE}} - \frac{U}{U_{LE}}\right)\mathrm{Tan}\,\alpha. \tag{13}$$

3.4. Intermittency

The intermittency at a point is defined as the proportion of time which the flow is turbulent at that point. For a two dimensional boundary layer however this intermittency is also equal to the proportion of a spanwise line, which passes through the same point, and is occupied by turbulent flow at a particular instant. Consider such a spanwise line, which is travelling downstream at the local spot trailing edge velocity U_{TE}. Fig. 5 shows that any spots initiated in the shaded x-t window will cross the spanwise line as it travels downstream through the distance Δx. It therefore follows that the spot generation rate per unit span

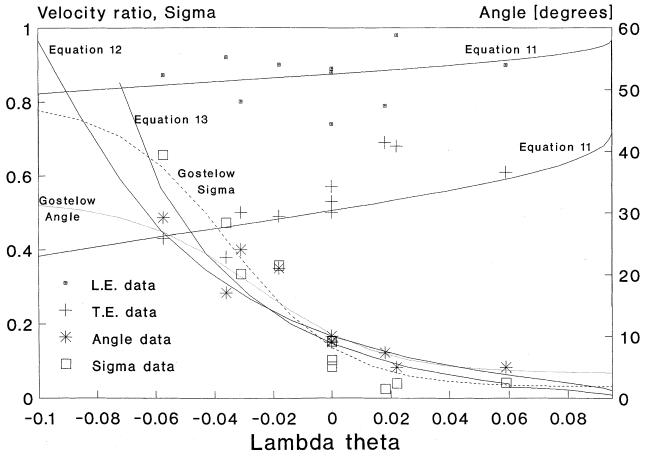

Fig. 4. Spot trailing and leading edge velocities, spreading half angle and propagation parameter.

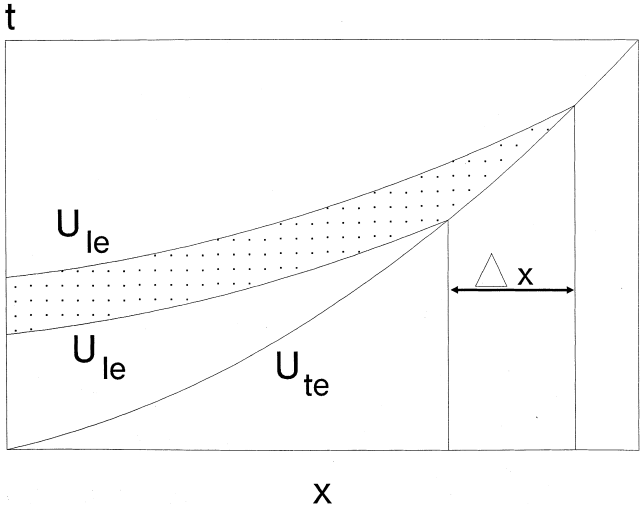

Fig. 5. Spot generation window for spanwise line travelling downstream at U_{TE}.

$$\frac{dN}{dt} = (1-\gamma)\left(\frac{U_{LE} - U_{TE}}{U_{LE}}\right)\int_0^x PU\left(\frac{z}{\ell}\right)^3 dx - \frac{2U_{TE}N^2\mathrm{Tan}\,\alpha}{1-\gamma}. \tag{14}$$

The first term in this equation represents the rate at which spots generated upstream arrive at laminar regions on the line. The second term represents the rate at which spots already on the line merge. The increase in intermittency is due to lateral spreading of spots on the line thus

Substituting Eq. (12) for α and

$$\frac{d\gamma}{dt} = 2NU_{TE}\mathrm{Tan}\,\alpha \tag{15}$$

$$\frac{dx}{dt} = U_{TE} \tag{16}$$

for the spanwise line, results in

$$\frac{dN}{dx} = \frac{(1-\gamma)\sigma}{U\mathrm{Tan}\,\alpha}\int_0^x PU\left(\frac{z}{\ell}\right)^3 dx - \frac{2N^2\mathrm{Tan}\,\alpha}{(1-\gamma)} \tag{17}$$

and

$$\frac{d\gamma}{dx} = 2N\,\mathrm{Tan}\,\alpha \tag{18}$$

Eqs. (17) and (18) have not been used previously in transition models for predicting intermittency. However, they are consistent with the frequently adopted Narasimha (1985) model. Narasimha assumed in his concentrated breakdown model that all turbulent spots originated at the start of transition location $x = x_s$. Thus

$$\int_0^x PU\left(\frac{z}{\ell}\right)^3 dx = 0 \quad \text{for } x < x_s$$
$$= n \quad \text{for } x \geqslant x_s. \tag{19}$$

He also assumed that the values of α and σ were constant. With these assumptions, Eqs. (17) and (18) can readily be reduced to the Narasimha intermittency equation

$$\gamma = 1 - \exp\left(\frac{-\sigma n(x - x_s)^2}{U}\right). \tag{20}$$

The recent work of Gostelow et al. (1995) presented in Fig. 4 clearly indicates that α and σ will vary greatly for

boundary layers with imposed streamwise pressure gradients. Solomon et al., 1995 accommodated this variation in their model whilst retaining Narasimha's assumption of concentrated breakdown. However, Johnson and Fasihfar (1994) have shown that the concentrated breakdown model itself leads to a different statistical distribution of turbulent spot size than that observed in experiments. They also demonstrated that their observed distributions were more closely represented by a distributed breakdown model such as the one adopted in this paper.

3.5. Boundary layer integral technique

In the current work, the development of the boundary layer is computed through numerical integration in the streamwise x direction of the boundary layer momentum equation

$$\frac{\mathrm{d}\theta}{\mathrm{d}x} = \frac{C_\mathrm{f}}{2} - \left(\frac{2\theta + \delta^*}{U}\right)\frac{\mathrm{d}U}{\mathrm{d}x}. \tag{21}$$

The laminar and turbulent portions of the boundary layer are integrated separately and the integral parameters are evaluated as intermittency weighted averages of the laminar and turbulent values. So:

$$\begin{aligned} C_\mathrm{f} &= (1-\gamma)C_\mathrm{fl} + \gamma C_\mathrm{ft}, \\ \mathrm{Re}_\delta* &= (1-\gamma)\mathrm{Re}_{\delta^* l} + \gamma\,\mathrm{Re}_{\delta^* \mathrm{t}}, \\ \mathrm{Re}_\theta &= (1-\gamma)\,\mathrm{Re}_{\theta l} + \gamma\,\mathrm{Re}_{\theta \mathrm{t}} \end{aligned} \tag{22}$$

The intermittency γ is obtained by numerical integration of Eqs. (17) and (18). The laminar boundary layer is assumed to have a Pohlhausen profile

$$\begin{aligned} \frac{u}{U} &= 2\frac{y}{\delta} - 2\left(\frac{y}{\delta}\right)^3 + \left(\frac{y}{\delta}\right)^4 \\ &\quad + \frac{\lambda}{6}\left[\left(\frac{y}{\delta}\right) - 3\left(\frac{y}{\delta}\right)^2 + 3\left(\frac{y}{\delta}\right)^3 - \left(\frac{y}{\delta}\right)^4\right]. \end{aligned} \tag{23}$$

Thus:

$$\frac{\theta}{\delta} = \frac{37}{315} - \frac{\lambda}{945} - \frac{\lambda^2}{9072} \tag{24}$$

and

$$\frac{\delta^*}{\delta} = \frac{3}{10} - \frac{\lambda}{120}. \tag{25}$$

If the laminar boundary layer separates, the Pohlhausen parameter λ is kept constant at -12 downstream of the separation point. A similar technique was adopted successfully by Solomon et al. (1995) for separated laminar flow.

When a laminar portion of the boundary layer becomes turbulent, then it follows from the conservation of momentum that

$$\theta_l = \theta_\mathrm{t} \tag{26}$$

The turbulent boundary layer integral parameters C_f, Re_θ and H were evaluated using the Ludwieg and Tillman (1950)

$$C_\mathrm{f} = 0.246(10)^{-0.678H}\,\mathrm{Re}_\theta^{-0.268} \tag{27}$$

and Goksel (1968)

$$\ln\left(\frac{H}{H-1}\right) = 0.1016\ln\mathrm{Re}_\theta + 0.4822 \tag{28}$$

relations.

4. ERCOFTAC test case results

The ERCOFTAC test cases (Savill, 1991) were established from measurements within two dimensional boundary layers developing on a flat plate. The first three cases (T3A-, T3A and T3B) were for nominally zero pressure gradient for three freestream turbulence levels of 1%, 3% and 6%. The remaining five test cases were for a pressure distribution along the plate typical of an aft loaded gas turbine blade. In the first of these (T3C1) the freestream turbulence level was 5%. For T3C2 to T3C5, where the turbulence level was 2.5%, the tunnel velocity was progressively reduced such that the transition location moves along the plate from the favourable pressure gradient region into the adverse pressure gradient region.

The model used in this paper requires knowledge of both the freestream turbulence level and its integral length scale. For the ERCOFTAC test cases, the measured freestream turbulence levels were used and the integral length scale was taken as 30% of the dissipative length scale provided by Savill at the plates leading edge. This length scale was assumed to increase with distance downstream according to Roach's (Roach, 1987) correlation.

4.1. Zero pressure gradient cases

4.1.1. Case T3A-

The freestream turbulence level for the T3A- test case is nominally 1% with a turbulent integral length scale at the plate leading edge of 2.0 mm. The predictions and measured values of skin friction coefficient and shape factor are shown in Figs. 6 and 7. Transition is predicted to start at $\mathrm{Re}_x = 800{,}000$ whereas it is observed at $\mathrm{Re}_x = 1{,}300{,}000$.

For this test case, the integral length scale at start of transition is almost equal to the boundary layer thickness. Earlier in this paper it has been shown that the boundary layer is most receptive to freestream turbulent wavelengths which are greater than approximately five times the boundary layer thickness and this is most marked at low skin friction coefficient. It therefore follows that, in this test case, transition results from the strong amplification of the longest wavelengths in the freestream, which here make up only a small proportion of the freestream turbulent energy. This can be demonstrated by decreasing the freestream integral length scale (by 40%) as shown in Fig. 6. This decreases the proportion of long wavelengths in the freestream and, as shown by Fig. 6, moves the start of transition Re_x downstream to the observed location. This improves the prediction of the experimental data, but it should be noted that a similar improvement could also be obtained by similar changes to the empirical constants, which are used to predict the receptivity of the boundary layer to low frequencies.

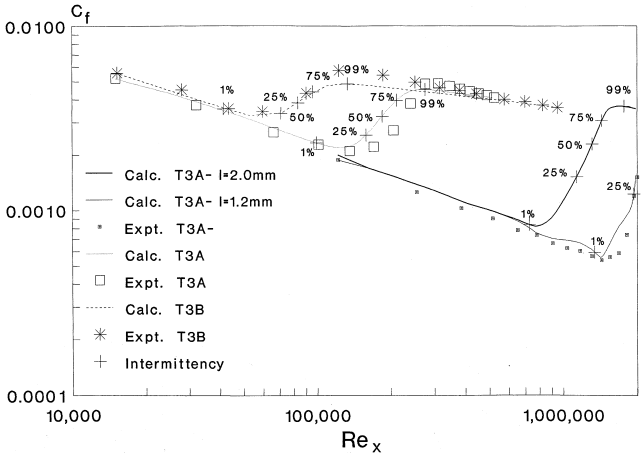

Fig. 6. Measurements and predictions of skin friction coefficient for the zero streamwise pressure gradient cases T3A-, T3A and T3B.

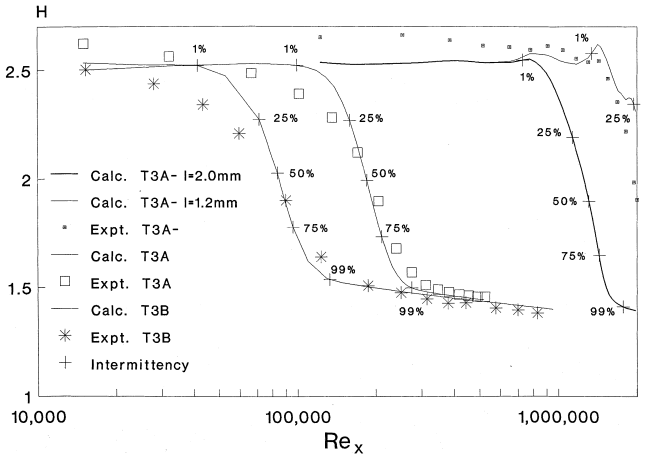

Fig. 7. Measurements and predictions of shape factor for the zero streamwise pressure gradient cases T3A-, T3A and T3B.

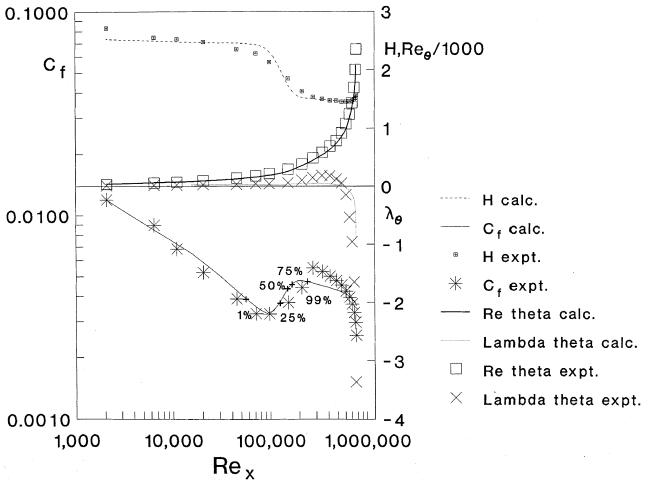

Fig. 8. Measurements and predictions for Re_θ, λ_θ, C_f and H for the T3C1 test case.

4.1.2. Case T3A

The freestream turbulence level for case T3A is approximately 3% and the integral length scale is 9.0 mm.

The predictions for T3A shown in Figs. 6 and 7 are fairly close to the measured values. However, the experiments show a decrease in H prior to start of transition whereas the predictions maintain the Blasius value of $H = 2.5$. Similar reductions in H due to a raised freestream turbulence level have been observed by several researchers (e.g., Johnson (1994), Gostelow et al. (1994)) and are believed to be due to enhanced mixing within the laminar boundary layer. Start of transition is predicted slightly early, but the transition length is very close to the measured value. The overshoot in the observed value of the skin friction coefficient beyond that for a fully developed turbulent boundary layer is not predicted, which is a usual failing of integral boundary layer methods (e.g., Gostelow et al. (1994)).

The integral length scale of 9.0 mm is approximately twice the boundary layer thickness at start of transition. The boundary layer is therefore receptive to the majority of the freestream turbulent frequencies and so the transition location is fairly insensitive to the integral length scale. The predicted Re_x values for $\gamma = 1\%$ and 99% are in fact increased by 5.3% and 7.5%, respectively if the length scale is reduced by 10%.

4.1.3. Case T3B

Case T3B has a nominal free stream turbulence level of 6% with an integral length scale of 12.5 mm which is six times the boundary layer thickness at start of transition. The transition location will therefore be unaffected by significant changes in the length scale. The computational results shown in Fig. 6 show that the location of the minimum C_f is predicted late, but once again the transition length is well represented.

4.2. Pressure gradient cases

4.2.1. Case T3C1

The turbulence grid used in the T3B case is also used in the T3C1 case to induce the turbulence level of approximately 5%. The integral length scale is 6.5 mm at the plate leading edge. Fig. 8 shows that the pressure gradient is mildly favourable up to $Re_x = 6 \times 10^5$ but then becomes strongly adverse. The favourable pressure gradient has the effect of delaying the predicted minimum C_f location from $Re_x = 62{,}000$ for case T3B to 100,000.

The start of transition is predicted fairly well, but transition appears to progress rather more rapidly than observed experimentally. This could be because of an overprediction in the spot generation rate or growth rate for a favourable pressure gradient. The development of Re_θ shown in the figure is nevertheless predicted accurately.

4.2.2. Case T3C5

The remaining four test cases are for a nominal freestream turbulence level of 2.5% induced by the T3A turbulence grid. The tunnel geometry and hence pressure coefficient distributions are the same as for case T3C1, but the tunnel speed is progressively reduced through cases T3C5, T3C2, T3C3 and T3C4, which has the effect of moving transition downstream.

For the T3C5 case, transition occurs within the favourable pressure gradient region and so the minimum C_f location is delayed to $Re_x = 230{,}000$ compared with $Re_x = 120{,}000$ for the zero pressure gradient case T3A. Fig. 9 shows that transition proceeds more slowly than observed. This could be because the spot generation rate or growth rate is underpredicted. However, the opposite effect was obtained for the favourable pressure gradient in case T3C1. A possible explanation for this may be that the skin friction coefficient value for the laminar boundary layer is predicted to be higher than the observed

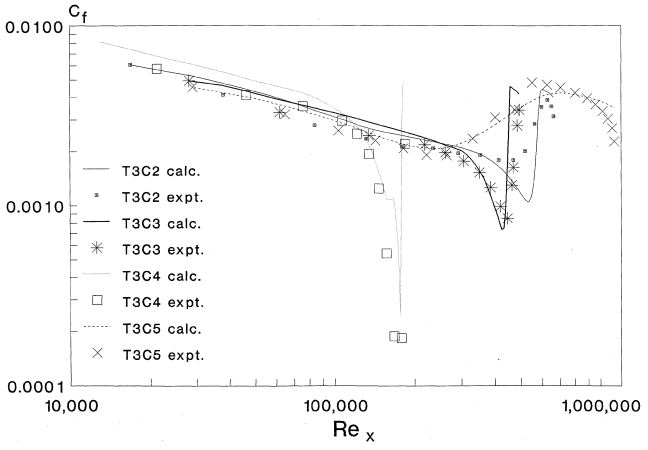

Fig. 9. Measurements and predictions of skin friction coefficient for the test cases T3C2, T3C3, T3C4 and T3C5.

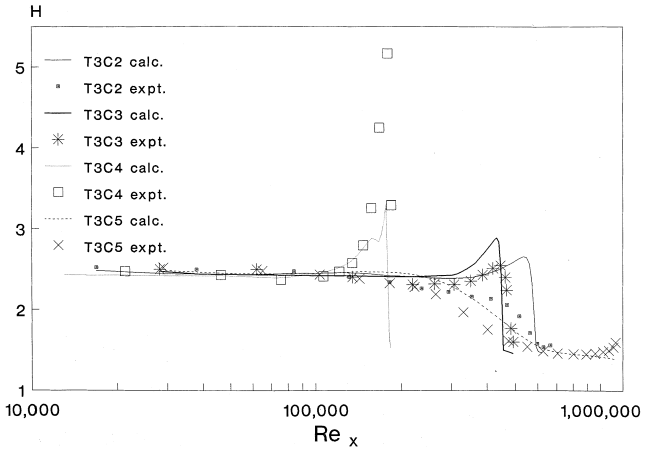

Fig. 10. Measurements and predictions of shape factor for the test cases T3C2, T3C3, T3C4 and T3C5.

value for case T3C5. This will lead to a low spot generation rate and hence a slower growth in intermittency.

4.2.3. Case T3C2

The tunnel velocity is reduced in case T3C2 such that although transition inception occurs within the favourable pressure gradient region, transition is only completed once the pressure gradient has become adverse. Fig. 9 shows that the minimum C_f location is predicted at $Re_x = 520{,}000$ whereas the experimental observations suggest this location is at about $Re_x = 430{,}000$. This means that when the almost laminar boundary layer enters the adverse pressure gradient at $Re_x = 470{,}000$, the predicted value of C_f drops rapidly and H increases (Fig. 10). The adverse pressure gradient does however rapidly accelerate the computed transition process and the end of transition is predicted close to the observed position at $Re_x = 620{,}000$.

4.2.4. Case T3C3

For this case, start of transition is observed early in the adverse pressure gradient region and transition is still not completed at the end of the plate. Fig. 9 shows that the boundary layer approaches laminar separation before the minimum C_f is reached at $Re_x = 420{,}000$, close to the experimental minimum. The predicted transition process proceeds more rapidly than observed however and transition is predicted to end prior to the end of the plate.

4.2.5. Case T3C4

For T3C4 the transitional boundary layer separates at $Re_x = 1.5 \times 10^5$ before reattaching as a turbulent boundary layer at $Re_x = 1.8 \times 10^5$. The current integral method is incapable of correctly predicting the boundary layer development beyond laminar separation. Nevertheless, the minimum C_f value and the subsequent rise through transition is predicted fairly well.

5. Gostelow test case results

Gostelow et al. (1992) have undertaken an extensive series of wind tunnel experiments to investigate the influence of freestream turbulence level and streamwise deceleration on transition. Various grids were placed 1200 mm upstream of the plate leading edge to induce freestream turbulence levels (measured at the leading edge) of 1.2, 2.1, 3.1, 3.9 and 5.4%. These levels were used for the current modelling work and were assumed to decay along the plate according to the Roach (1987) correlation. Thus

$$Tu = Tu_o\left(1 + \frac{x}{x_o}\right)^{-5/7}. \tag{29}$$

Roach's correlation was also used to determine the integral length scale

$$\frac{\ell}{d} = 0.2\left(\frac{x + x_o}{d}\right)^{-1/2}, \tag{30}$$

from grid bar diameters given by Gostelow et al. (1992). Calculations were not attempted for the no grid case ($Tu = 0.3\%$) where Tollmien–Schlichting instability would lead to transition rather than the bypass mode modelled here.

A hinged roof to the wind tunnel was used to produce the adverse pressure gradients. The streamwise velocity gradients induced are therefore given by

$$\frac{1}{U}\frac{dU}{dx} = \text{Constant}. \tag{31}$$

Calculations were performed for 11 values of this constant (0 to 2 at 0.2 increments) for each turbulence level with a leading edge freestream velocity of 10 m/s.

Gostelow defined his start and end of transition position by using the Narasimha (1985) $F(\gamma)$ procedure whereby Eq. (20) is fitted through the $\gamma = 25$–75% data and then extrapolated to the $\gamma = 0\%$ (start) and 99% (end) positions. This procedure minimises the uncertainties involved in measuring intermittency. For consistency, the same procedure was adopted here for the model results.

5.1. Zero pressure gradient results

The predicted and measured Re_θ start and end of transition values are plotted in Fig. 11. The start of transition is

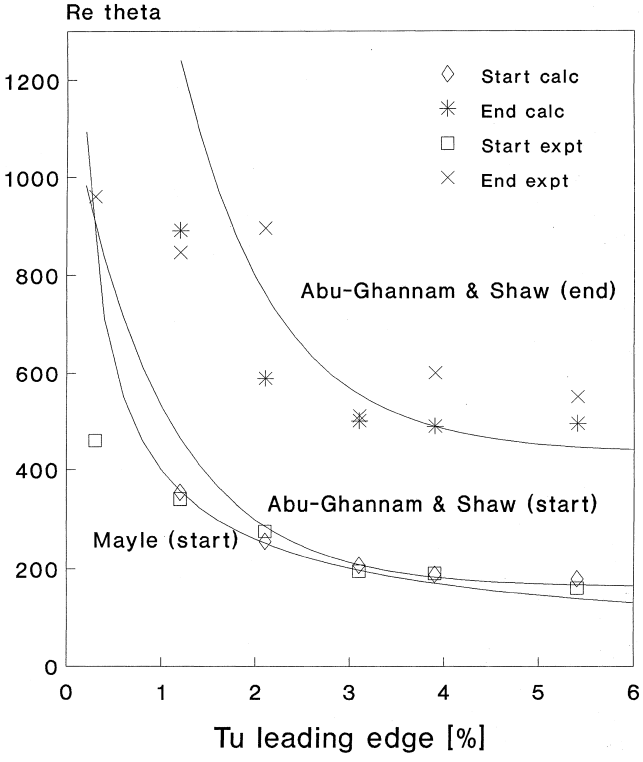

Fig. 11. Comparison of measurements, empirical correlations and model predictions for zero pressure gradient.

accurately predicted by both the model and the Mayle (1991) correlation. The Abu-Ghannam and Shaw (1980) correlation also gives reliable predictions except for the Tu = 1.2% case. A likely reason for this is that Abu-Ghannam and Shaw used a tunnel where the turbulence grid was only 750 mm upstream of the plate leading edge. This results in a shorter integral length scale and hence transition inception occurs later at the lowest turbulence levels. The effect of length scale is therefore believed by the authors to be responsible for the discrepancies between empirical correlations at low freestream turbulence levels. The inclusion of the effects of length scale in the current model should therefore improve prediction at low turbulence level. The accuracy of the predictions for end of transition is difficult to judge because of the greater degree of scatter in the experimental data. The predicted Re_θ values are generally rather lower than measured however. Nevertheless the predictions are rather more accurate than the Abu-Ghannam and Shaw correlation for all but the Tu = 2.1% case.

5.2. Adverse pressure gradient results

The start of transition results are presented in Fig. 12. Both the Abu-Ghannam and Shaw correlation and the present calculations are reasonably accurate for the turbulence levels of 3.1%, 3.9% and 5.4%; however, the current prediction is superior at the lowest turbulence level. The calculations indicate a slightly larger effect from the pressure gradient than observed in the measurements, particular at the higher turbulence which is consistent with the predictions for the ERCOFTAC test cases. One reason for this may be that Roach's correlations for turbulence level and length scale used here were formulated for zero pressure gradients. They may therefore be inaccurate when a pressure gradient is present. The experimental results for end of transition (Fig. 13) suggest that the effect of turbulence level is much reduced in an adverse pressure gradient. This is because intermittency increases in an adverse pressure

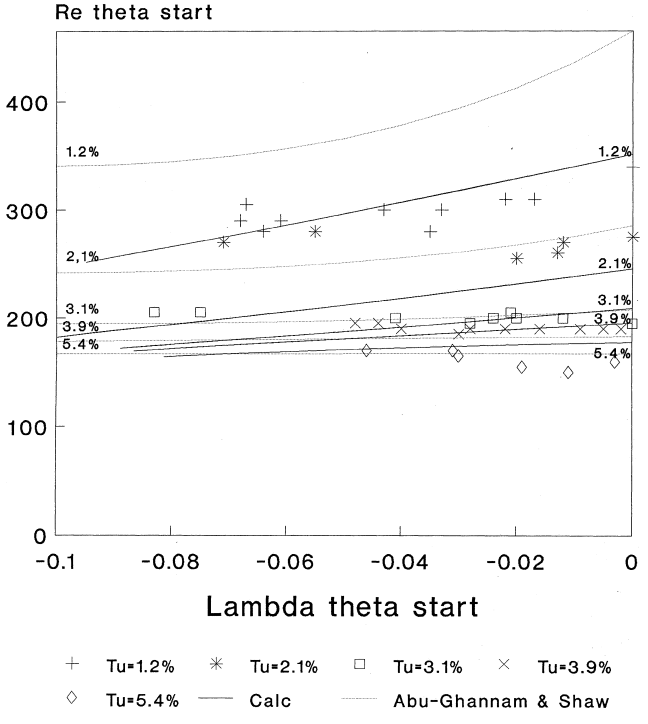

Fig. 12. Comparison of start of transition Re_θ measurements and model predictions for adverse pressure gradients.

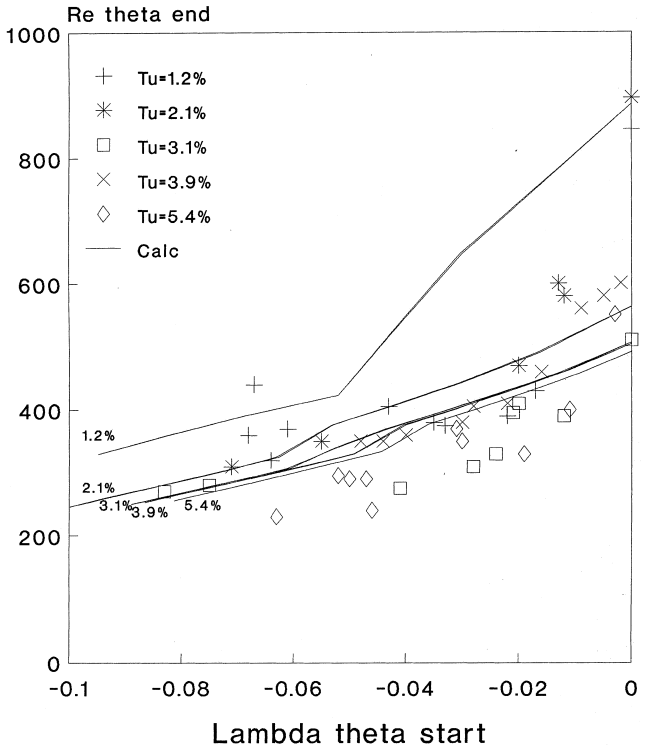

Fig. 13. Comparison of end of transition Re_θ measurement and model predictions for adverse pressure gradients.

gradient primarily due to the rapid growth of existing spots with a large spreading angle (Fig. 4) rather than through the generation of further spots. Freestream turbulence level only affects spot generation, but not their subsequent growth. The end of transition is predicted fairly well, for all except the Tu = 1.2% case, where the transition length is predicted to be too long for moderate pressure gradient where λ_θ is between -0.05 and -0.01. One possible explanation for this discrepancy is that transition at that turbulence level is largely through a T-S mechanism rather than the bypass mode modelled here. T-S waves increase the number of velocity minima and hence the rate of spot generation resulting in a reduced transition length.

The correlations for end of transition provided by Abu-Ghannam and Shaw were found to over-estimate the Re_θ end value by over 100% for the strongest adverse pressure gradients. A better correlation has been provided more recently by Walker and Gostelow (1990). By consideration of the T-S wavelength, they established a minimum transition length

$$Re_{Tran\ min} = 2.3\ Re_{\delta*s}^{1.5}. \tag{32}$$

An empirical correlation was then established to relate the minimum transition length to the actual length

$$\frac{Re_{Tran}}{Re_{Tran\,min}} = 9.412\ \exp(-3121\lambda_{\theta s}\ \ell n(Tu) + 33.692\ \lambda_{\theta s} + 0.248\ \ell n(Tu)). \tag{33}$$

This transition length was computed using the Abu-Ghannam and Shaw start of transition correlation values for $Re_{\delta s}^*$ and is plotted in Fig. 14. For the Tu = 3.1%, 3.9% and 5.4% cases, the transition length is overestimated by the correlation but is reasonably accurately determined by the authors' calculation procedure. The measured transition length for Tu = 2.1% is approximately double the length of all the other cases and these results lie close to the correlation. Both the correlation

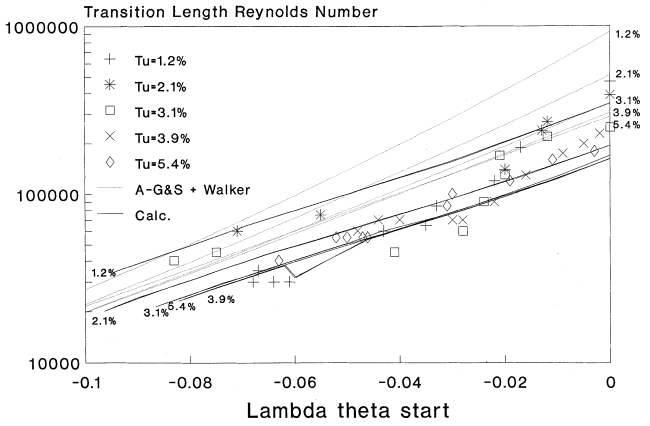

Fig. 14. Comparison of transition length measurements, empirical correlations and model predictions for adverse pressure gradients.

and authors' prediction result in transition lengths greater than those measured for the Tu = 1.2% case. Once again, it is believed that there is significant T-S activity for this case which is not accounted for in the authors' model and thus the transition length is overpredicted.

An alternative method of comparing transition lengths is to consider Narasimha's Dimensionless Spot Parameter N_N (Narasimha, 1985) which is plotted in Fig. 15. Both Gostelow's experimental data and the current predictions indicate an increase by a factor of approximately 100 in this parameter with increasing pressure gradient. There is however a much larger observed variation with turbulence level than predicted. For turbulence levels above 1.2%, the experimental results are reasonably represented by the predictions when the degree of experimental scatter (particularly for the Tu = 3.1% case) is taken into account. The higher values measured for Tu = 1.2% (and Tu = 0.3% which was not predicted) are attributable to T-S activity increasing the spot generation rate.

5.3. Intermittency

Gostelow and co-workers plotted measured intermittency values against the dimensionless distance ξ. One such plot is shown in Fig. 16 together with the Narasimha (1985) Eq. (20) and the current prediction. Dhawan and Narasimha (1958) considered distributed breakdown, but found that concentrated breakdown modelled their early intermittency data most

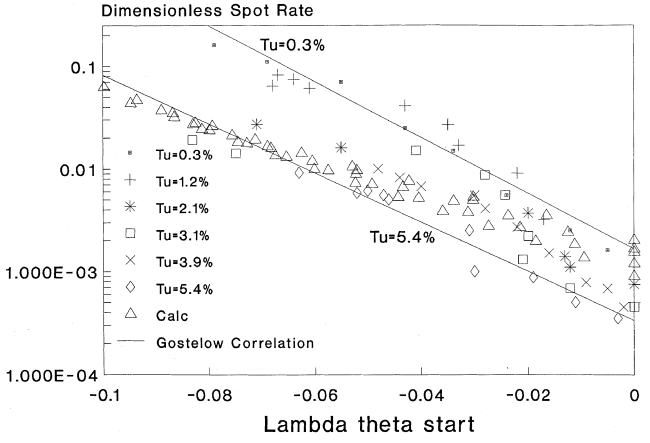

Fig. 15. Measured and predicted Narasimha spot parameter.

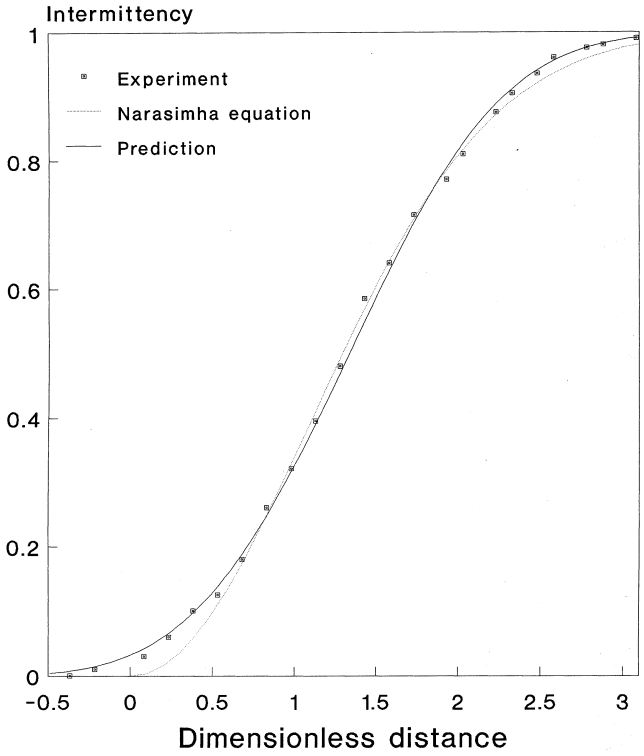

Fig. 16. Measured and predicted intermittency for the Tu = 2.1% zero pressure gradient case.

accurately. Increase in intermittency beyond this point is then entirely due to the subsequent growth in the spots initiated at $\xi = 0$. However, the much more recently measured intermittencies shown in Fig. 16 deviate from this curve both at low and high intermittencies. Johnson and Fasihfar (1994) measured the statistical properties of spot length through transition and showed that these were better predicted by a distributed breakdown model, similar to the current one, rather than the Narasimha concentrated breakdown model. This deduction is confirmed by the more accurate prediction of intermittency by the current distributed breakdown model shown in Fig. 16.

6. Conclusions

1. A model for the generation of turbulent spots and their growth is presented. The model is dependent on the nature of the near wall velocity fluctuations and hence on the receptivity of the boundary layer to freestream turbulence. Experimental observations indicate that the boundary layer is most receptive to low frequency perturbations and thus it is these low frequencies which dominate the transition process.

2. The current model predicts start of transition with similar accuracy to empirical correlations. End of transition is predicted more reliably by the model, particularly at higher freestream turbulence. The over-prediction of transition length at Tu < 1.5% is most likely due to significant Tollmien–Schlichting activity which is not accounted for in the current model. The Narasimha spot propagation parameter is also accurately predicted for all but the Tu < 1.5% case.

3. At low turbulence levels, where the integral length scale is similar in magnitude to the boundary layer thickness, the transition length and location are highly dependent on the integral length scale. For moderate turbulence levels, the

integral length scale is approximately twice the boundary layer thickness and the transition is only moderately sensitive to length scale. At the highest turbulence levels, the transition process is independent of the length scale which is now many times larger than the boundary layer thickness.

4. The development of intermittency through transition is predicted considerably better by the current distributed breakdown model than by the Narasimha concentrated breakdown model.

7. Future work

Although the current transition model has significantly reduced the number of empirical constants required to predict spot generation (only three constants are required in Eq. (1)), a significant number of constants are still required (Eqs. (11) and (12)) to predict spot growth. A future objective is to derive theoretical models both for the laminar boundary layer response to freestream turbulence and for spot growth in order to reduce the number of empirical constants further. This should lead to improved reliability of the model particularly for predicting flows where lack of empirical data makes the empirical correlations inaccurate.

Acknowledgements

The authors acknowledge ASME for permission to publish, in this paper, material contained within the authors' ASME conference papers 96-GT-444 and 97-GT-475.

References

Abu-Ghannam, B.J., Shaw, R., 1980. Natural transition of boundary layers – the effects of turbulence, pressure gradient and flow history. J. of Mech. Eng. Sci. 22, 213–228.

Dhawan, S., Narasimha, R., 1958. Some properties of boundary layer flow during the transition from laminar to turbulent motion. J. of Fluid Mechanics 3, 418–436.

Fasihfar, A., Johnson, M.W., 1992. An improved boundary layer transition correlation. ASME paper 92-GT-245.

Goksel, O.T., 1968. Some effects of spherical roughness upon the incompressible flow of a boundary layer with zero pressure gradient. Ph.D. thesis, University of Liverpool.

Gostelow, J.P., Blunden, A.R., Walker, G.J., 1992. Effects of free-stream turbulence and adverse pressure gradients on boundary layer transition. ASME J. of Turbomachinery 116, 392–404.

Gostelow, J.P., Hong, G., Walker, G.J., Dey, J., 1994. Modelling of boundary layer transition in turbulent flows by linear combination integral method. ASME Paper No. 94-GT-358.

Gostelow, J.P., Melwani, N., Walker, G.J., 1995. Effects of streamwise pressure gradient on turbulent spot development. ASME J. of Turbomachinery 118, 737–743.

Hinze, J.O., 1959. Turbulence – Introduction to its Mechanism and Theory. McGraw Hill, New York.

Johnson, M.W., 1994. A bypass transition model for boundary layers. ASME J. of Turbomachinery 116, 759–764.

Johnson, M.W., Fasihfar, A., 1994. Properties of turbulent bursts in transitional boundary layers. Int. J. of Heat and Fluid Flow 15 (4), 283–290.

Ludwieg, H., Tillman, W., 1950. Investigation of the wall shear stress in turbulent boundary layers. NACA T.N. 1284.

Mayle, R.E., 1991. The role of laminar-turbulent transition in gas turbine engines. ASME J. of Turbomachinery 113, 509–537.

Mayle, R.E., Schulz, A., 1996. The path to predicting bypass transition. ASME paper 96-GT-199.

Narasimha, R., 1985. The laminar-turbulent transition zone in the boundary layer. Prog. in Aerospace Science 22, 29–80.

Roach, P.E., 1987. The generation of nearly isotropic turbulence by means of grids. Int. J. of Heat and Fluid Flow 8 (2).

Savill, A.M., 1991. A synthesis of T3 test case predictions. Proc. 1st ERCOFTAC Workshop, Cambridge University Press, Cambridge.

Steelant, J., Dick., E., 1994. Modelling of by-pass transition with conditioned Navier–Stokes equations and a K-ϵ model adapted for intermittency. ASME paper 94-GT-12.

Solomon, W.J., Walker, G.J., Gostelow, J.P., 1995. Transition length prediction for flows with rapidly changing pressure gradients. ASME J. of Turbomachinery 118, 185–209.

Voke, P.R., Yang, Z., 1993. Numerical studies of the mechanisms of bypass transition in the flat plate boundary layer. Proceedings of 9th Symposium on Turbulent Shear Flows, Kyoto, Japan.

Voke, P.R., 1995. Laminar/turbulent transition of boundary layer influenced by free-stream disturbances, Euromech 330, Prague.

Walker, G.J., Gostelow, J.P., 1990. Effects of adverse pressure gradients on the nature and length of boundary layer transition. ASME J. of Turbomachinery 112, 196–205.